Materials Science & Engineering A 813 (2021) 141174

Contents lists available at ScienceDirect

Materials Science & Engineering A

journal homepage: http://www.elsevier.com/locate/msea

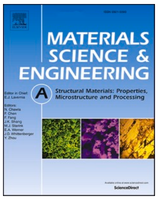

Thermally stable Al conductor prepared from Al powder with a low oxygen content

Cunguang Chen [a,b,c,*], Feng Li [d], Weihao Han [a], Tianxing Lu [a], Pei Li [a], Qianyue Cui [a], Yanli Sui [b], Zhimeng Guo [a,c], Alex A. Volinsky [e]

[a] *Institute for Advanced Materials and Technology, University of Science and Technology Beijing, Beijing, 100083, PR China*
[b] *State Key Laboratory for Advanced Metals and Materials, University of Science and Technology Beijing, Beijing, 100083, PR China*
[c] *Innovation Group of Marine Engineering Materials and Corrosion Control, Southern Marine Science and Engineering Guangdong Laboratory (Zhuhai), Zhuhai, 519000, PR China*
[d] *Guangxi Beibu Gulf New Materials Co. Ltd., Beihai, 536000, PR China*
[e] *Department of Mechanical Engineering, University of South Florida, 4202 E. Fowler Ave., ENG 030, Tampa, FL, 33620, USA*

ARTICLE INFO

Keywords:
Al conductor
Powder metallurgy
Thermal stability
Mechanical properties
Electrical conductivity

ABSTRACT

The high thermal stability of pure Al conductors is an urgent requirement for their applications in power transmission lines. Powder metallurgy (PM) Al conductor was produced in this work from Al powder with a low oxygen content (~0.1 wt%), followed by cold isostatic pressing, sintering, hot extrusion, and cold drawing. The microstructure evolution, mechanical properties and electrical conductivity of hot-extruded rods and cold-drawn wires before and after annealing at 300 °C and 500 °C were investigated. The γ-Al_2O_3 nanoparticles located primarily at high angle grain boundaries promote the stabilization of Al grains, resulting in enhanced annealing strength (89 MPa), almost twice higher than commercial pure Al (45 MPa). Fine grains and texture play a significant role in the overall strength (160 MPa) of PM Al conductors. One interesting finding is that the electrical conductivity of cold-drawn wires (60.2% IACS) is higher than the hot-extruded rods (58.7% IACS) due to the beneficial evolution of initial Al_2O_3 film and grain boundaries. The compatibility of documented strength-structure Hall-Petch relation was discussed. Optimal properties (172 MPa ultimate tensile strength and 60.2% IACS electrical conductivity) were obtained through cold drawing. These results push forward the potential application of PM Al in heat resistant conductors.

1. Introduction

Due to the low density, relatively high intrinsic conductivity, excellent corrosion resistance, and lower cost of aluminum (Al) [1,2], pure Al and Al alloys are used, including one or more layers of the 1350-H19 Al in the outer areas of aluminum conductor steel reinforcement (ACSR) used in the overhead conductor lines [3]. Electrical conductivity and strength are the most significant properties of metallic conductors, since good electrical conductivity can reduce electrical loss and improve transmission efficiency, and the high strength can help withstand the dead weight, wind, and ice loads. Unfortunately, the electrical conductivity and strength are usually mutually exclusive in metallic conductors [4,5].

Various approaches to enhance the mechanical performance of aluminum have been put forward to extend its application range. On the one hand, the strength can be greatly improved by adding alloy elements to produce the precipitation strengthening effect. Alloying with a low fraction of Mg and Si is a common method to manufacture wires in electrical engineering, resulting in an improved ultimate tensile strength in the 250–330 MPa range. However, since Mg and Si solute atoms could cause lattice distortions which markedly scatters electrons, the Al–Mg–Si conductive materials have lower electrical conductivity in the 57-52% IACS (International Annealed Copper Standard) range [1,6,7]. On the other hand, to further increase the strength of Al and Al alloys without dramatically degrading electrical conductivity, many reports have recently proposed severe plastic deformation (SPD) techniques, for instance, accumulated roll bonding (ARB), equal channel angular pressing (ECAP), high-pressure torsion (HPT) and cold drawing. In particular, for the pure Al without precipitates, SPD processes are the effective strategies to break the trade-off relation between the strength

---

[*] Corresponding author. Institute for Advanced Materials and Technology, University of Science and Technology Beijing, Beijing, 100083, PR China.
E-mail address: cgchen@ustb.edu.cn (C. Chen).

https://doi.org/10.1016/j.msea.2021.141174
Received 11 September 2020; Received in revised form 16 February 2021; Accepted 22 March 2021

and the electrical conductivity through the strengthening mechanisms of grain-boundary strengthening, dislocation strengthening, and texture strengthening [5,8–11].

Currently, the demand for a higher transmission capacity of electricity has elevated the operating temperature of the overhead conductor wires. Consequently, it is apt to cause the recovery and recrystallization, decrease of the dislocation density, and coarsening of grains and precipitates in the Al-based overhead transmission lines subjected to SPD, resulting in the decrease of the mechanical strength [7]. To increase the service temperature, the addition of Sc, Zr, Ce, La, Er, and other alloying elements are investigated to generate thermal-resistant precipitates to stabilize the microstructure [12–16]. For example, adding Sc and Zr forms $Al_3(Sc, Zr)$ precipitates, increasing the highest working temperature of the Al-0.2Sc-0.04Zr alloy to 345 °C [14]. However, the preparation process of these Al-RE (RE stands for rare earth) alloys is complicated, and the Al and RE elements are prone to segregation because of the huge difference in their melting point and density. Furthermore, for industrial applications, the overall production costs increase progressively with alloying, especially for these Al-RE materials including precious elements.

Li et al. proposed a sustainable ‘plain’ approach to obtain advanced metallic materials with a bespoke performance by engineering defects while reducing the materials’ compositional complexity [17,18]. Powder metallurgy (PM) Al may be taken as the ‘plain’ material because it is generally consolidated by gas atomized pure Al powder without alloying [19]. It is confirmed that PM Al shows superior mechanical properties and creep performance at elevated temperatures, which benefit from the homogeneously nanoscale γ-Al_2O_3 dispersoids originated from the native amorphous Al_2O_3 (am-Al_2O_3) films [20]. Also, flake powder metallurgy has been developed to fabricate biomimetic Al_2O_3/Al composites [21–23] with an excellent tensile strength of 262 MPa and 22.9% plasticity. However, the relevant electrical conductivity was not reported. These reports of PM Al are in stark contrast to the above Al and Al alloys such as Al–Mg–Si and Al-RE that are hardened by precipitates, solid solutions, or grain boundaries.

So far, the mechanical properties and electrical conductivity of the PM Al conductors have been rarely reported on. In the present research, PM Al conductors were prepared by cold isostatic pressing and sintering, followed by hot extrusion and cold drawing. In order to evaluate the thermal stability of PM Al expected to be applied at elevated temperatures, the tensile tests and electron backscatter diffraction (EBSD), and transmission electron microscopy (TEM) observations were carried out before and after annealing at ultra-high temperatures, i.e. 300 °C and 500 °C. The related strengthening mechanisms were also discussed. Finally, microstructure control through processing of PM Al results in a good combination of enhanced mechanical strength, extremely high thermal stability, and sufficient electrical conductivity.

2. Materials and methods

2.1. Materials

Nitrogen gas-atomized Al powders supplied by the Angang Group Aluminum Powder (AGAP) Co., Ltd., China were the starting materials in this study. Fig. 1 displays the powder morphology with the particle size distribution. The raw powder particles have a nearly spherical shape and 20 μm median particle diameter, which was determined using a laser diffraction system (BT-9300S) by wet dispersion. The inductively coupled plasma-atomic emission spectrometry (ICP-AES) was used to analyze the chemical composition of the Al powder, which is Al 99.83 wt %, Fe 0.086 wt%, Si 0.039 wt%, and Cu 0.001 wt%. The Al powder particles were passivated by exposure to air to obtain a thin oxide layer, the thickness of which is 2–4 nm, as demonstrated in previous work [20, 24]. The nominal oxygen content in the Al powder was 0.1 wt% (data supplied by AGAP Co., Ltd.).

2.2. Samples preparation

The powders were pre-pressed into green bodies (90 mm in diameter, 300 mm in height) by cold isostatic pressing (CIP) at 180 MPa and then subjected to vacuum sintering at 610 °C for 180 min. After that the sintered cylindrical ingots were hot extruded at 380 °C into Al bars with a diameter of 12 mm. Since commercial pure Al conductors (CPACs) are often made by a standard cold-drawing route, the investigation of the mechanical properties and the microstructure evolution of cold-drawn Al wires is significantly important referring to previous research [5,25, 26]. The cold-drawing experiment on the hot-extruded PM Al rods was conducted using a bull block drawing machine. The hot extrusion and cold drawing were performed in the air. The PM Al wire with a diameter of 3 mm was manufactured by cold drawing for 11 passes from the original Al rod, which was hot extruded. The total area reduction was about 93.7%. While strength degradation is a natural phenomenon commonly occurring at the increased operating temperature during the service of traditional Al conductors, it is important to investigate the strength degradation of the annealed PM Al materials. Therefore, to study the thermal stability of the extruded PM Al rods, air annealing at 300 °C and 500 °C for 24 h was applied, i.e., below and above extrusion temperature, respectively. The cold-drawn PM Al wire of 3 mm in diameter was annealed in air at 300 °C for 24 h. The schematic diagram of the preparation process of the investigated samples is shown in Fig. 2.

2.3. Characterization

The uniaxial tensile tests of the hot-extruded and cold-drawn PM Al before and after annealing were carried out using the WDW-200D testing machine according to the ASTM-E08 standard. A wire-cut electric discharge machine was used to prepare standard dog-bone tensile

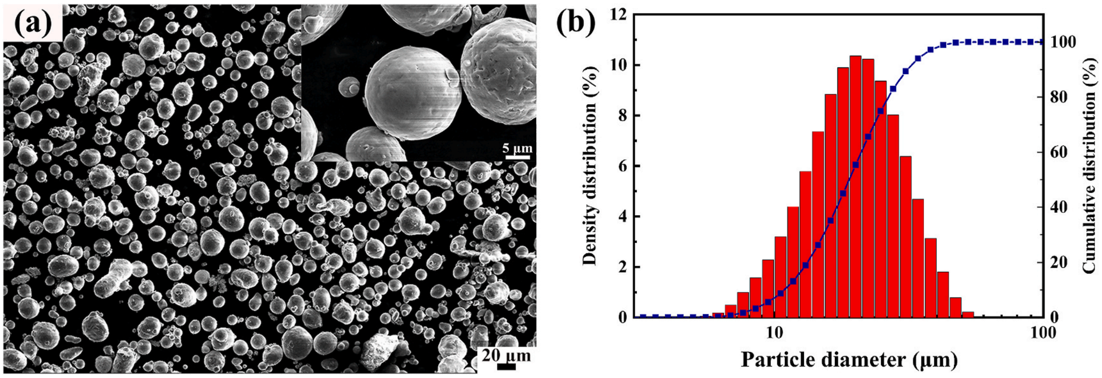

Fig. 1. (a) SEM image of Al powder and (b) the particle size distribution.

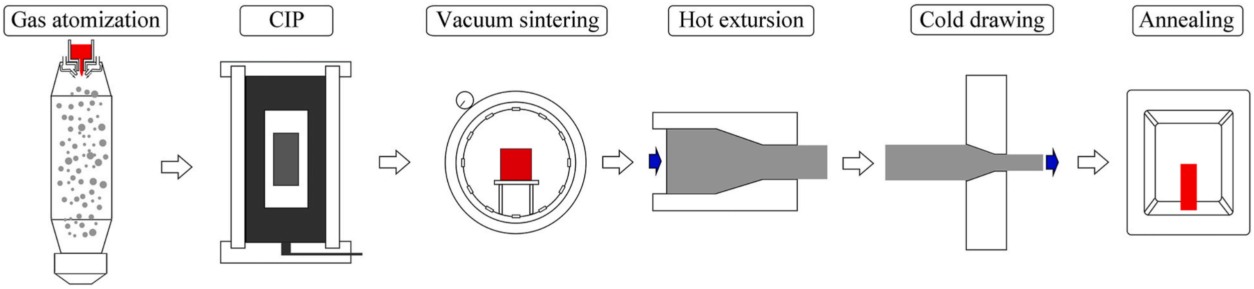

Fig. 2. Schematic diagram of the preparation process of investigated samples.

samples for hot-extruded PM Al with a gauge diameter of 5 mm and a gauge length of 25 mm. The tensile samples for cold-drawn PM Al were cut with a gauge length of 150 mm. All the tensile specimens were tested at room temperature and a constant strain rate of 10^{-3} s^{-1} with the tensile axis parallel to the extrusion and drawing direction. Five tests were performed for each sample, and average values were taken.

The electrical conductivity of the specimens with the 2 mm × 2 mm × 40 mm dimensions was measured using the four-probe method with the TH2513A DC low resistance tester. In order to ensure the accuracy of the results, the room temperature was adjusted to about 20 °C by the air conditioner during the measurement process. At least five measurements were made, and the average values and standard deviation were calculated.

Al pieces with a thickness of 1 mm cut from the radial section and the axial section of the hot-extruded, cold-drawn, and annealed PM Al specimens were made into samples for EBSD observations. Sample preparation for EBSD was done by grinding with SiC paper up to 2000 grit and then electrolytically polished using an etching solution containing 10 vol% perchloric acid and 90 vol% alcohol at −20 °C for 8 s. The grain orientation distribution and the texture evolution were measured by the EBSD technique integrated into a field emission scanning electron microscope (FESEM, ZEISS SUPRA™ 55). TEM samples were cut from the cross-section of cold-drawn Al wires, ground to a thickness of 0.05 mm, and then twin-jet electropolished using a solution of 20 vol% perchloric acid and 80 vol% methanol. TEM foils were examined by the FEI Tecnai G2 F30 microscope operating at 200 kV. The three-dimensional atomic probe (3DAP, LEAP 5000XR) was used to analyze the spatial distribution of oxygen and aluminum elements. The samples were wire-cut to the 0.5 mm × 0.5 mm × 1.5 mm size, and the needle tip of less than 100 nm was micro-polished by 2 vol% perchloric acid and 98 vol% ethylene glycol monobutyl ether.

3. Results and discussion

3.1. Microstructure of consolidated Al bulk

The SEM microstructure and EDS results of PM Al cylindrical ingots sintered in a vacuum are shown in Fig. 3. Fig. 3a presents residual pores as the black regions with white margins in the sintered Al bulk. Because of these defects not being compact, the Al sintered bulk only achieves 97.5% of the Al theoretical density measured according to the Archimedes principle, which is consistent with prior findings adopting the nitrogen sintering [19]. Moreover, the morphology of the initial Al powder particles surrounded by chain-typed γ-Al_2O_3 dispersoids is visible. In line with the previous reports [20,24], the transformation from am-Al_2O_3 platelets to γ-Al_2O_3 dispersoids occurred after sintering at 610 °C. Also, the white margins as part of the prior particle boundaries (PPBs) in the sintered SEM microstructure can be regarded as oxygen-rich area via the EDS analysis in Fig. 3b and c. On the one hand, because of the sintered bulk large size, the sintering process is completed before all the air retained in the green compact is fully expelled by pulling a vacuum, more oxides will be formed around the pores coupled with the low surface energy. On the other hand, some oxides may be generated from the chemical reaction between the etching solution containing perchloric acid and Al matrix during the electrolytic polishing in the preparation of SEM samples.

To characterize the microstructure in terms of the grain size, texture, and stress distribution of sintered Al bulk after CIP, the EBSD observations in Fig. 4 were carried out. As revealed in the orientation image map (OIM) of the grains in Fig. 4a, the structure shows no obvious preferred grain orientation. It can be also found in the inverse pole figures (IPFs) in Fig. 4e that there is a little difference between the maximum value (2.07) and the minimum value (0.26) of the pole density. During the process of CIP, spherical Al powders first go through the particle rearrangement and then are subjected to plastic deformation under the isostatic pressure of 180 MPa because the metals such as Al with the face-centered cubic (FCC) crystal structure are easy to deform. However, the recrystallization takes place as the sintering process goes on, leading to the formation of Al grain structure containing the majority of completely developed crystal grains bound by high angle grain boundaries (HAGBs) higher than 15° marked by red color (Fig. 4b). There are only a couple of sub-grains confined to low angle grain boundaries (LAGBs) marked by white color (2–15°), which are concentrated on PPBs in Fig. 4c. The emergence of LAGBs indicates that a few substructures are produced despite undergoing the stage of high temperature (610 °C) sintering for PM pure Al. Corresponding to the map of kernel average misorientation (KAM) in Fig. 4d, the location of LAGBs exhibits the high density of geometrically necessary dislocations (GNDs)

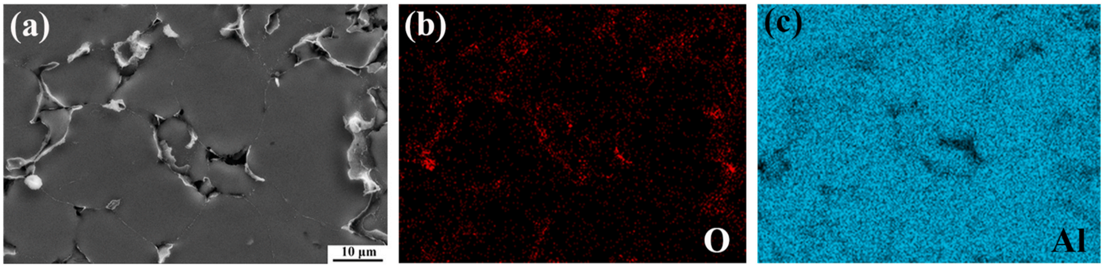

Fig. 3. (a) SEM microstructure and (b, c) EDS results of as-sintered PM Al in a vacuum. The EDS results in (b, c) represent oxygen and aluminum elements distribution, respectively.

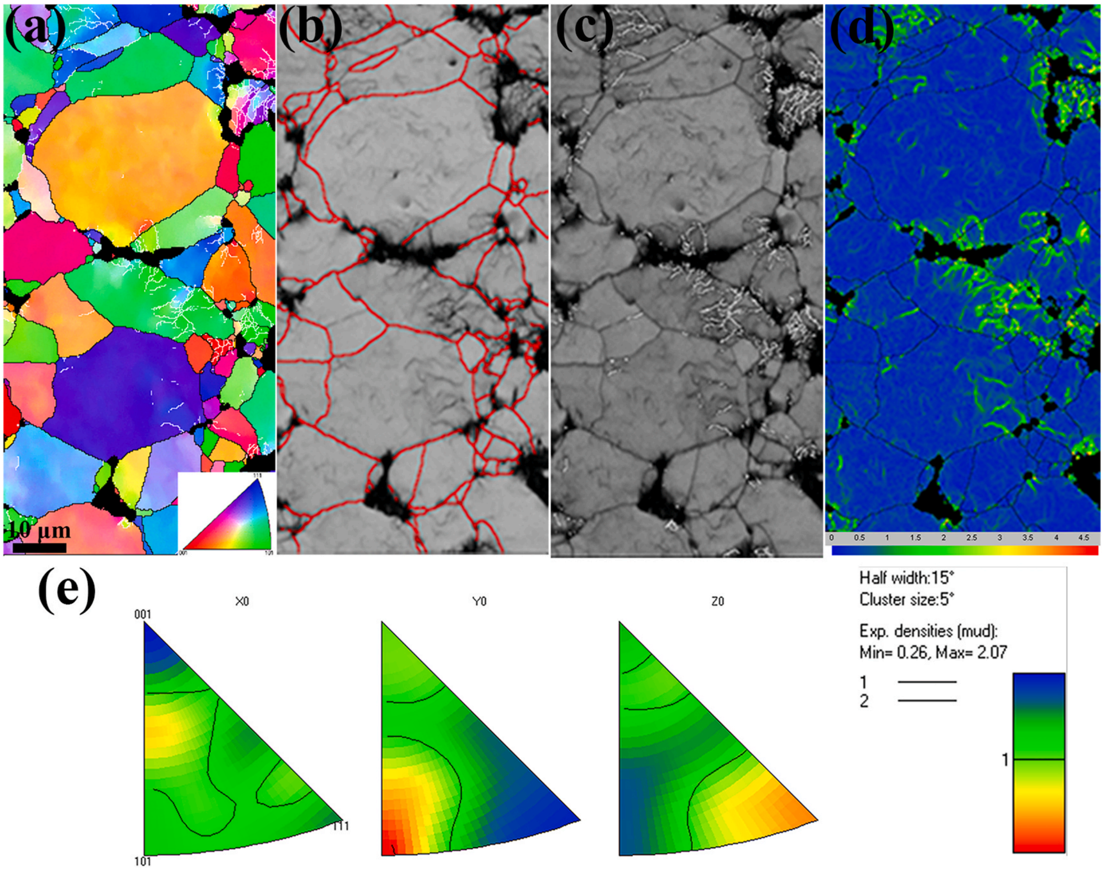

Fig. 4. EBSD microstructure with grains, texture, and stress distribution of vacuum sintered Al: (a) the orientation image map of grains, (b) the map of high angle grain boundaries, (c) the map of low angle grain boundaries, (d) the map of kernel average misorientation, and (e) the inverse pole figures.

in green color, representing the area of intense deformation. The stress level at the boundary is higher than inside the particle. These phenomena should be attributed to as-formed γ-Al_2O_3 dispersoids as strong obstacles to the dislocation motion around the PPBs. Nevertheless, in terms of the Al_2O_3 component including am-Al_2O_3 platelets and γ-Al_2O_3 dispersoids, the sintering is severely hampered, leading to the formation of pores illustrated in Fig. 3a.

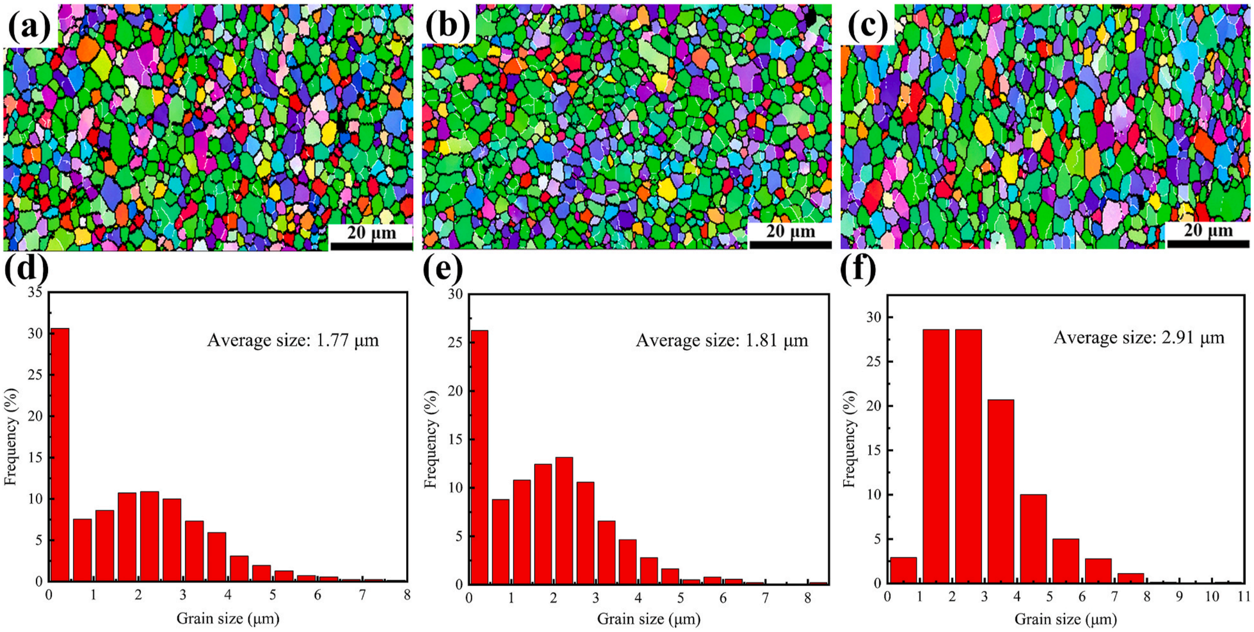

Fig. 5. (a–c) Grain orientation image maps and (d–f) grain size distribution of PM Al rods in the radial direction (a) after hot extrusion, (b) annealed at 300 °C and (c) 500 °C for 24 h. The bar graphs (d–f) correspond to (a–c), respectively.

3.2. *Microstructure of hot extruded and annealed PM Al*

Since the grain is an important factor that influences various properties, the changes of the grains in the radial direction are characterized by EBSD. Fig. 5 shows grain OIMs and grain size distribution of the hot-extruded Al rods before and after annealing at 300 °C and 500 °C for 24 h, respectively, determined by EBSD and analyzed by the Channel 5 software integrated into the ZEISS SUPRA™ 55 SEM. The overall grain size observed from the radial section in Fig. 5a–c is relatively uniform, and no abnormally large grains are found, even for the microstructure annealed at 500 °C in Fig. 5c. The average grain size of the hot-extruded Al rods annealed at 300 °C for 24 h (1.81 μm in Fig. 5e) is almost equal to the hot-extruded Al rods (1.77 μm in Fig. 5d). However, with the increase of annealing temperature, the average grain size gradually increases to 2.91 μm (Fig. 5f) for the HE Al rods annealed at 500 °C for 24 h. As calculated, the grain size after annealing at 500 °C for 24 h is 60% higher than after annealing at 300 °C for 24 h, and 64% higher than that before annealing. Nevertheless, the grains annealed at 500 °C still keep an even and small appearance compared to the previous reports on the cast Al ingot followed by deformation [5].

Now that the grain size has changed after annealing at the evaluated temperature, the factors such as recovery and recrystallization that cause the change of grain characteristics should be taken into account. Fig. 6 demonstrates the microstructure evolution of hot-extruded and annealed Al rods in the axial direction by the EBSD technique. Among the EBSD maps, the blue, yellow, and red regions represent the recrystallization microstructure, substructure, and deformation microstructure, respectively. The statistical results related to the volume fraction of these three kinds of microstructure is given in Table 1. Each measurement was performed three times and the average values are reported with the relative error not exceeding 5%. As for the hot-extruded Al rods, it is seen in Fig. 6a that the red zone covers most of the viewed area, while the blue one occupies a very small proportion, that is, most of the grains accounting for 62.9% are still deformed along with 11.8% recrystallization microstructure and 25.3% substructure. It is widely reported that Al has relatively high stacking fault energy and the dislocations tend to dynamically recover due to the dominating wavy slip mode in the hot working above the recrystallization temperature of Al (380 °C in this study) [27,28]. The dislocation density in substructures is low, and the stored residual energy is insufficient to cause dynamic recrystallization. Therefore, in the hot extrusion process of this study, the proportion of recrystallization that occurred is relatively low (11.8%). However, after subsequent annealing at 300 °C below the extrusion temperature for a long time (24 h), the proportion of recrystallization increased to 44.9%, whereas the deformed region dropped sharply to 3.5%, as seen in Fig. 6b. After raising the annealing temperature to 500 °C for Al, as seen in Fig. 6c, more than half of the investigated microstructure (53.8%) has completed recrystallization, and the deformed microstructure almost disappeared, only leaving 1.6% according to the statistical results. Besides, unlike the dramatic change of the recrystallization and deformed microstructure, the substructure only takes 51.6% and 44.6% even after undergoing prolonged annealing at 300 °C and 500 °C, respectively. The microstructure of hot-extruded PM Al presented herewith is described corresponding to the TEM characterization of the as-processed PM Al and after annealing at the same conditions reported previously [19].

Table 1
Statistical results of recrystallization, substructure, and deformation areas.

Material	Recrystallization area	Substructure area	Deformation area
Hot-extruded	11.8%	25.3%	62.9%
300 °C annealed	44.9%	51.6%	3.5%
500 °C annealed	53.8%	44.6%	1.6%

The texture produced by plastic deformation can be considered as one of the strengthening factors in metallic materials [5,25,29]. In this study, the extrusion ratio, calculated as the reduction of the sample diameter from 90 mm to 12 mm exceeds 56%. The texture evolution and the corresponding volume fraction of the <111> texture in the hot-extruded and annealed PM Al rods are given in Fig. 7. The orientation distribution maps of the PM Al rods observed from the radial section in Fig. 7a–c show that the rods have a weaker <001> fiber texture together with a stronger <111> fiber texture, which are typical textures in the FCC metals with large deformation. The volume fraction of the <111> texture demonstrated in Fig. 7d–f is calculated as:

$$f_{<111>} = S_{<111>} / S_0 \tag{1}$$

Here, $f_{<111>}$ is the volume fraction of the <111> texture, $S_{<111>}$ is the area of the subgrains with <111> orientation and S_0 is the measured total area. After annealing at 300 °C for 24 h, there is a slight change in the <111> texture with the volume fraction decrease from 67.2% to 68.1%. However, an increasing amount of subgrains with the <001> orientation and a decreasing amount of subgrains with the <111> orientation can be found in the PM Al rods annealed at 500 °C for 24 h, indicating the occurrence of texture evolution from the <111> texture to the <001> texture. It can be estimated that the volume fraction of the <111> texture in the 500 °C annealed rods drops to 53%, smaller than the hot-extruded rods.

As for the evolution of the <001> recrystallization texture in axisymmetrically deformed FCC metals, such as aluminum in this work, it is typically described in terms of the two models. On the one hand, Inoue et al. [30] showed that it could be explained by the strain-induced grain boundary migration (SIGM) model. It is claimed that the <001> region is adjacent to the <111> oriented region and that subgrains in the <001> region recover faster, i.e., the subgrain coalescence or the subgrain growth occurs at the very early stage of the recrystallization process. Since the <001> subgrains are larger than the <111> subgrains, the <001> subgrains are assumed to be the nuclei for recrystallization which could grow into the <111> region through the migration of the high-angle grain boundaries between the <111> and <001> regions. Despite the SIGM model being usually observed in lightly deformed metals, the process of hot extrusion followed by sintering (Fig. 4) in this study is very different from drawing with large deformation by Inoue et al. [30]. This may explain the slight increase in the volume fraction of the <111> texture after 300 °C annealing, as previously mentioned in Fig. 7e. On the other hand, according to the calculations of the SERM

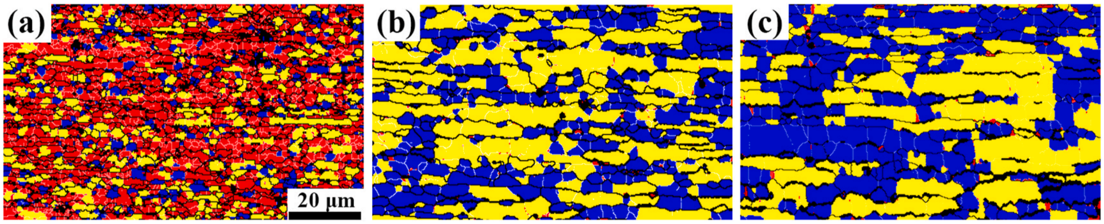

Fig. 6. EBSD microstructure evolution of PM Al rods in the axial direction (a) after hot extrusion, (b) annealed at 300 °C and (c) 500 °C. In the EBSD maps, the blue, yellow, and red regions are denoted as the recrystallization microstructure, substructure, and deformation microstructure, respectively. (For interpretation of the references to color in this figure legend, the reader is referred to the Web version of this article.)

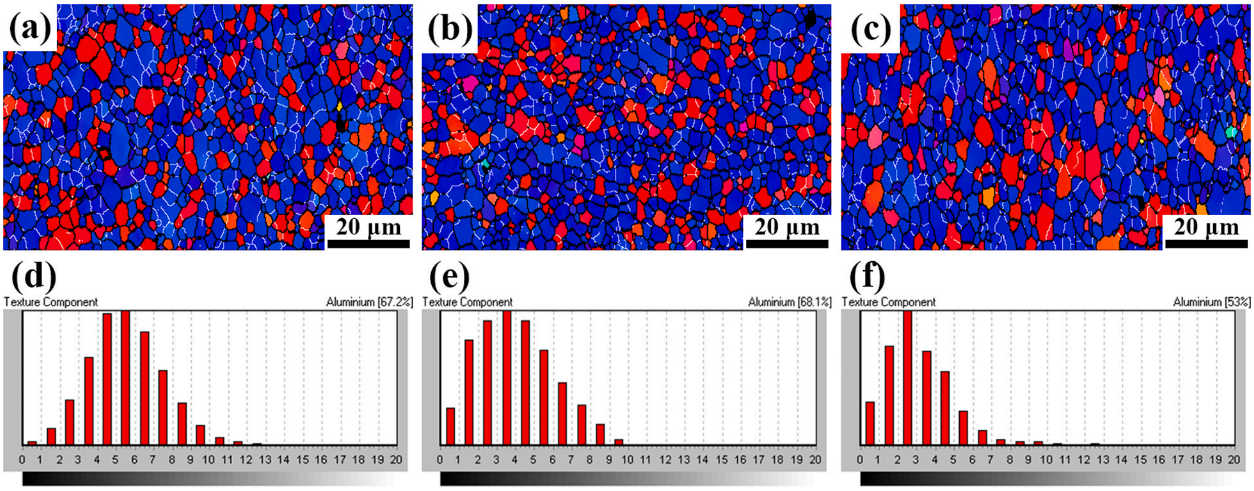

Fig. 7. (a–c) Texture evolution and (d–f) the corresponding volume fraction of the <111> texture (blue regions) in the PM Al rods in the radial direction after (a, d) hot extrusion, (b, e) annealing at 300 °C, and (c, f) annealing at 500 °C. (For interpretation of the references to color in this figure legend, the reader is referred to the Web version of this article.)

model proposed by Lee [31], the <111> and <001> components in the deformation texture are going to transform into the <001> component after recrystallization. For the <111> oriented crystal, three m<110> directions and the planes made by the slip directions are calculated to be active slip systems. The absolute maximum principal stress direction will become the minimum elastic modulus direction of recrystallized grains to minimize the strain energy of the system. The minimum elastic modulus directions of aluminum are the <001> directions. Therefore, the deformed <111> grains will be replaced by the recrystallized <001> grains. Also, the <001> oriented grains might retain their

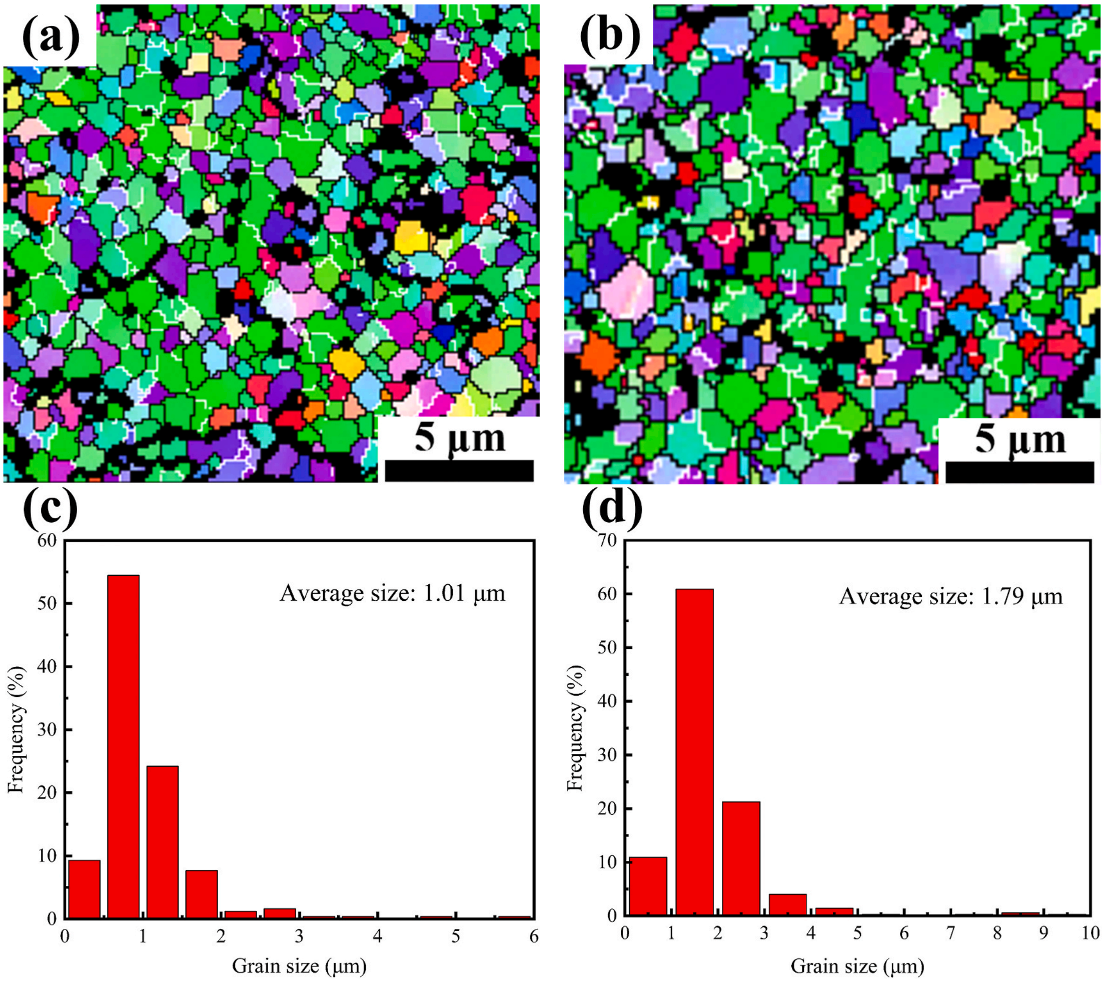

Fig. 8. (a, b) Grain orientation image maps and (c, d) grain size distribution of PM Al wires as (a, c) cold-drawn and (b, d) subsequently annealed at 300 °C.

deformation texture during annealing by continuous recrystallization by recovery-controlled processes without long-range high-angle boundary migration, leading to the growth of the <001> grains at the expense of their neighboring <111> grains, which tend to assume the <001> orientation. Consequently, it is understandable that the volume fraction of the <111> texture obtained in Fig. 7f after prolonged annealing at high temperature (500 °C) is declined.

3.3. *Microstructure of cold drawn and annealed PM Al*

Fig. 8 shows the grain OIMs and grain size distributions of the PM Al wire with a diameter of 3 mm cold drawn and annealed at 300 °C for 24 h. As illustrated in Fig. 8, the average grain size of the cold-drawn PM Al wire in the radial direction is 1.01 μm (Fig. 8c), whereas the grains grow up to 1.79 μm (Fig. 8d) after annealing. Even if the increase of grain size reaches 77.2%, the average size of annealed grains remains at a relatively fine level above the recrystallization temperature. As reported in Ref. [25], the commercially pure Al conductor (CPAC) of 2.98 mm in diameter was prepared by cold-drawing via 9 passes from the original Al rod with a diameter of 9.5 mm, and the total area reduction was 90.2%, very close to 93.7% in this study. Subject to annealing at 300 °C for 20 min, it was observed that the subgrains gradually grew from 0.4 μm of the cold-drawn CPAC to 1.9 μm after annealing at 300 °C for 20 min, with the sharp increase of 325%.

As reported in Ref. [18], the naturally formed nanoscale Al_2O_3 on the surface of the Al powder is thermodynamically stable even at 500 °C. Compared with the commercial pure Al, the most striking difference for the studied PM Al is the γ-Al_2O_3 dispersoids solidly located in the HAGBs per TEM observations (Fig. 9), so that PM Al can still maintain a relatively fine and uniform structure at a higher temperature. For one, the Al_2O_3 particles with the size of 50–100 nm (Fig. 9a) are distributed on the subgrain boundaries, and the spacing between them is measured to be 200 nm. The 30 nm Al_2O_3 particle is captured in Fig. 9b. At the same time, as seen from the high-resolution image (Fig. 9c), the strongly tight interface is observed at the boundary between the γ-Al_2O_3 particle and the Al matrix. By measuring the radius of multiple diffraction rings from the selected area electron diffraction (SAED) in Fig. 9d, it is determined that the nearly spherical and white particles in Fig. 9a and b are γ-Al_2O_3 with the hexagonal crystal structure, comparing the data of the standard PDF card (#2310-0173) and previous studies.

Most importantly, the characteristics of γ-Al_2O_3 in three-dimensional space are first confirmed by the 3DAP measurements demonstrated in Fig. 10. In terms of the element distribution analysis in the spatial scale of ϕ60 nm × 100 nm, it is found that a red surface encompassing region is superimposed on the point cloud, revealing the presence of an oxygen-rich cluster within the data. The oxygen element is clumped together into a flat shape and possess the 3D size of 15 nm × 20 nm × 30 nm with the comprehensive analysis of Fig. 10a–c. It can be considered that oxygen has no solid solubility in Al at experimental temperature. Thus, the oxygen-rich cluster can be seen as a γ-Al_2O_3 area rather than random fluctuations in the solid solution. Understandably, the size of γ-Al_2O_3 observed by 3DAP is not quite identical with the TEM results, because γ-Al_2O_3 particles observed by TEM and 3DAP are usually in different zones. However, the size of γ-Al_2O_3 particles obtained by 3DAP is consistent with the TEM results of Fig. 9b and the previous research (28.2 nm) [20]. Clusters of AlO are discovered in Fig. 10d, which is the

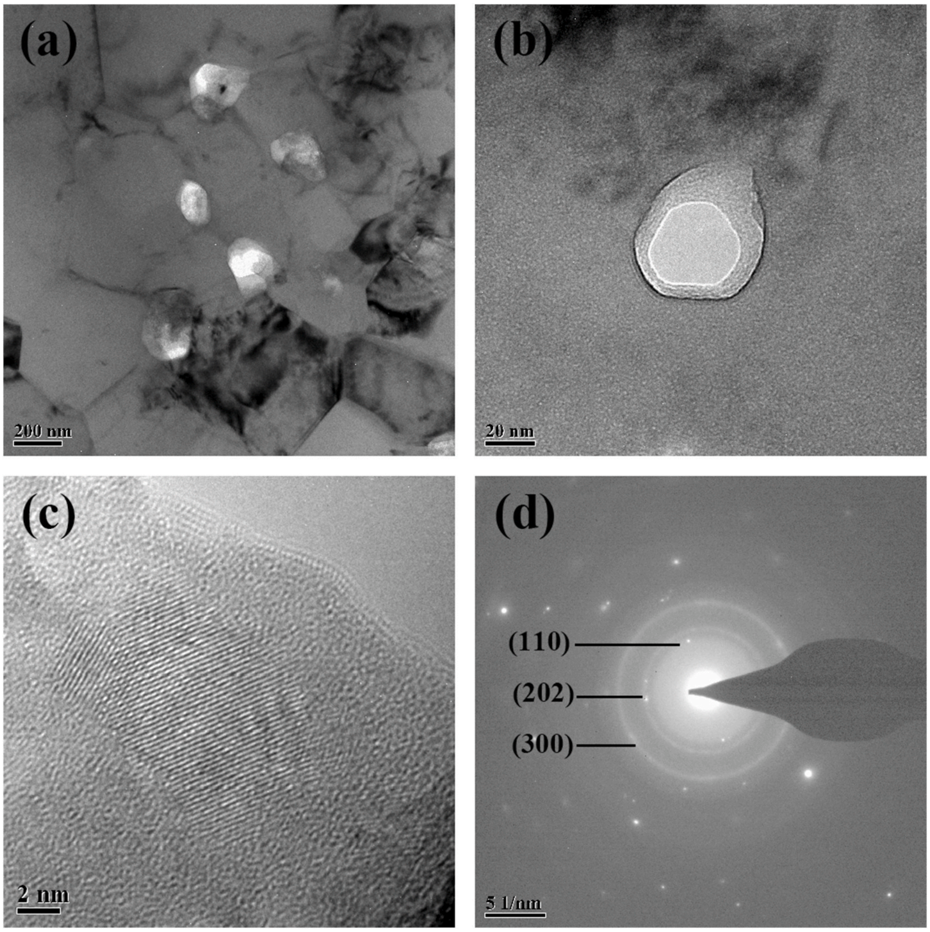

Fig. 9. TEM images of γ-Al_2O_3 dispersoids: (a) 50–100 nm γ-Al_2O_3 (white particles), (b) 30 nm γ-Al_2O_3 (white particle), (c) lattice fringe image of γ-Al_2O_3 in high-resolution mode, indicating tight interface between γ-Al_2O_3 and Al matrix, and (d) the selected area electron diffraction.

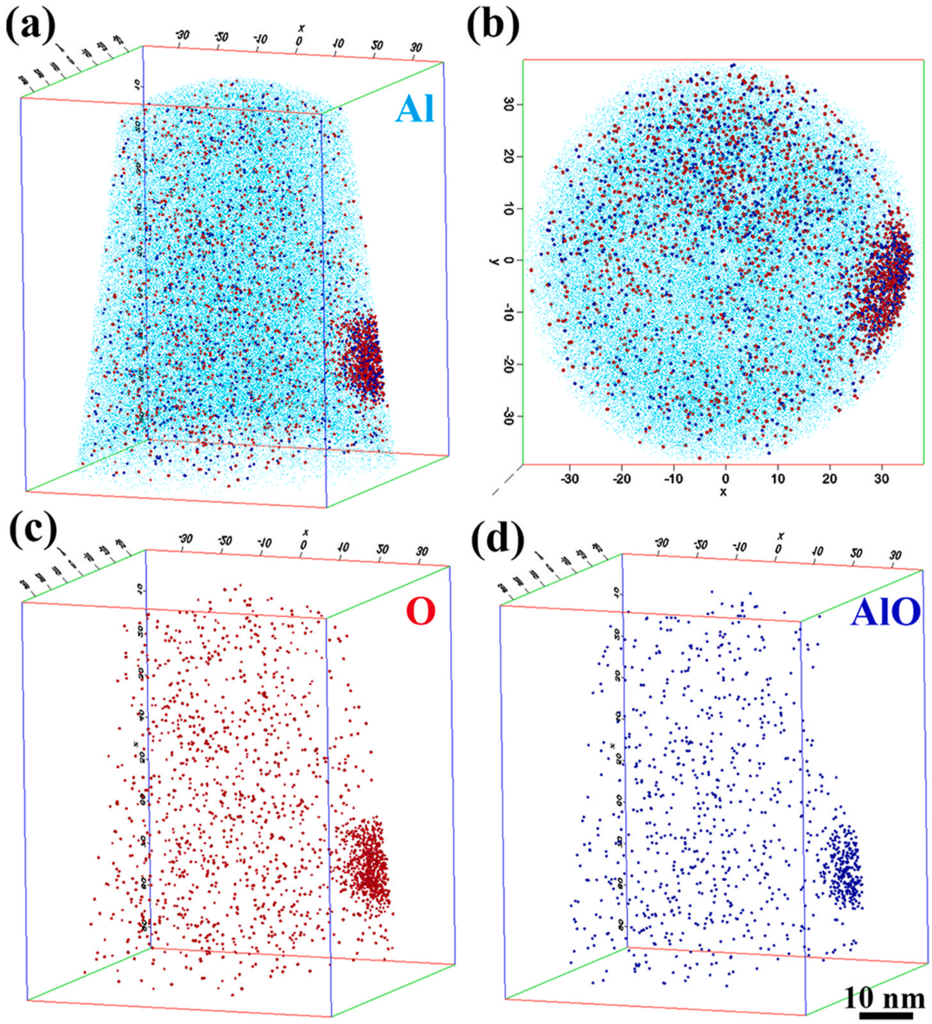

Fig. 10. Spatial element distribution of: (a) Al, side view; (b) Al, top view; (c) oxygen and (d) AlO obtained by the 3DAP technique.

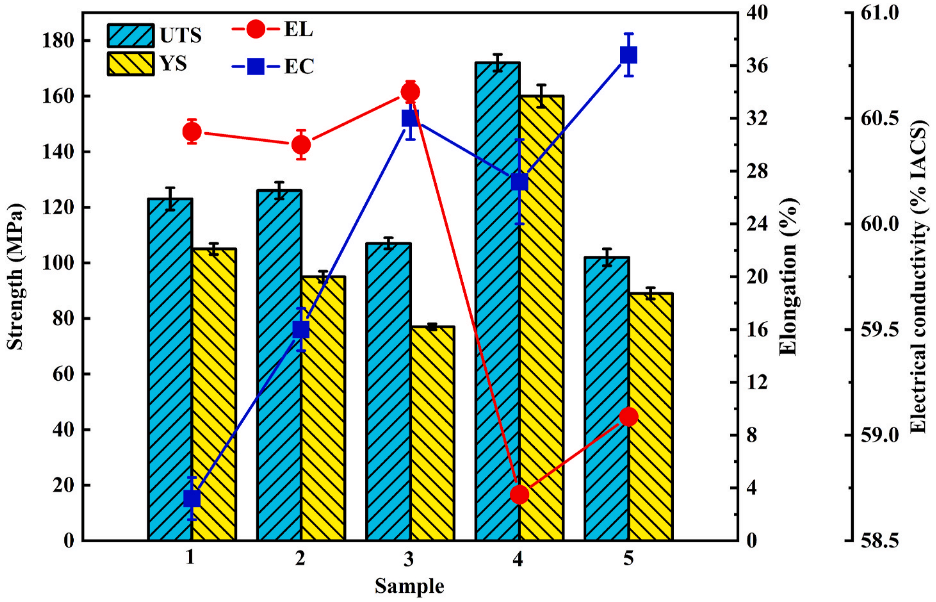

Fig. 11. Ultimate tensile strength (UTS), yield strength (YS), elongation (EL), and electrical conductivity (EC) of PM Al at different conditions: hot extrusion (Sample 1) and annealed at 300 °C (Sample 2) and 500 °C (Sample 3), cold drawn (Sample 4) and annealed at 300 °C (Sample 5).

subject of further investigation. Such findings are of particular interest and are not reported yet.

3.4. Mechanical properties and electrical conductivity

The ultimate tensile strength (UTS), YS, elongation, and electrical conductivity (EC) of PM Al at different conditions are shown in Fig. 11. Compared to the hot-extruded PM Al, the UTS of hot-extruded PM Al after annealing at 300 °C is almost unchanged and decreases by 13% after 500 °C annealing. The reduction in YS after annealing at 300 °C and 500 °C is about 9% and 37%, respectively. After annealing at 300 °C, the elongation shows no obvious change but increases slightly after annealing at 500 °C. In the case of cold-drawn PM Al wires with a diameter of 3 mm, a significant increase occurs in both UTS and YS. To be specific, the UTS is up to 172 MPa, which is a 40% increase compared with the extrusion state. The 52% YS increase is obtained. The increase of the YS is higher than UTS. When annealed at 300 °C, the UTS was 102 MPa, while the YS was 89 MPa. It can be calculated that the YS degradation (44%) is a little higher than UTS (41%).

With respect to the high-temperature stability of the microstructure and properties of Al conductors, the previous research [25] has demonstrated that the grain size of CPAC increased from 0.4 μm to 1.9 μm, or 375% after 20 min annealing at 300 °C, and the corresponding YS decreased to 70 MPa as listed in Table 2. Also, the YS of CPAC sharply decreased to 45 MPa when the holding time was prolonged to 12 h. In stark contrast, despite annealing for 24 h at 300 °C, the grain size of cold-drawn PM Al changed from 1.01 μm to 1.79 μm, increasing by 77%. The sample YS of 89 MPa after annealing is twice as high as CPAC, and the annealing holding time of PM Al is double that of CPAC. It can be concluded that the stability at the evaluated temperature PM Al is much higher than CPAC. It is worth noting that the reported CPAC contains 0.4% impurities, Si 0.11%, Fe 0.25%, Cu 0.01% and Mn < 0.03%, which could bring about stronger solution strengthening than PM Al in this study with 99.83% Al. Thus, it follows that the dominant factor stabilizing the microstructure and properties of PM Al should be the pinning of γ-Al_2O_3 particles at grain boundaries.

This viewpoint has been confirmed by numerous studies [20,24,32–35], including our previous results by rotary swaging on PM Al [19]. However, Balog et al. [35] and Schneibel et al. [36] have pointed out that the γ-Al_2O_3 particles located at HAGBs did not contribute dramatically to the room-temperature strengthening of the Al + γ-Al_2O_3 materials with the grain size ranging from 0.57 μm to 2.99 μm, within which the size of studied grains falls precisely, whereas grain boundaries played a significant role in the overall strength. In addition, the oxygen content of 0.1 wt% in PM Al stands for a small quantity of γ-Al_2O_3 particles, not enough to activate notable Orowan strengthening. Motivated by the above discussion, more conclusive strengthening mechanisms will be further identified.

The electrical conductivity of PM Al rods and wires is presented with square symbols in Fig. 11. The electrical conductivity of PM Al wires by a cold drawing (60.2% IACS) is higher than PM Al rods made by hot extrusion (58.7% IACS). This is an interesting phenomenon. Generally, the volume fraction of grain boundaries, the number of point defects, and the dislocation density increase during the cold drawing, which would enhance the electron scattering and increase electrical resistivity. However, for PM Al, the continuous Al_2O_3 film coated on the surface of Al powder is gradually drawn into long strips and eventually into particles, as seen in Fig. 9a during the process from hot extrusion to cold drawing. It is known that Al_2O_3 is an insulator. Thus, it is only when Al_2O_3 films become very small particles that the scattering of electrons is reduced, that is, the electrical conductivity will increase. Furthermore, the interactions between the electrons and the grain boundaries could lead to a decrease in electrical conductivity. Previous studies [25,29] have shown that the electrical resistivity caused by the grain boundaries nearly perpendicular to the axial direction should be much greater than that caused by ones parallel to the axial direction. As the degree of deformation increases, the grains will be stretched out longer. This means an increase of the grain boundaries parallel to the axial direction, resulting in the advancement of electrical conductivity. It is logical for the cold-drawn PM Al wires to have higher electrical conductivity, compared with hot-extruded PM Al rods. In addition, after annealing, the electrical conductivity of samples in both states (hot extrusion and cold drawing) is improved. Contributions to the resistivity added by dislocations and grain boundaries should gradually decrease with annealing temperature due to reduction of dislocation density and grain growth, respectively, thus leading to an increase of the electrical conductivity.

Table 2
Grain size (*d*) and mechanical properties of PM Al in the study and CPAC [26].

Material	CPAC			PM Al	
	Cold drawn	Cold drawn +300 °C/20 min annealed	Cold drawn +300 °C/12 h annealed	Cold drawn	Cold drawn +300 °C/24 h annealed
d (μm)	0.4	1.9	—	1.01 ± 0.08	1.79 ± 0.10
UTS (MPa)	210 ± 2	~90 ± 4	~85 ± 3	172 ± 3	102 ± 3
YS (MPa)	198 ± 2	~70 ± 4	~45 ± 7	160 ± 4	89 ± 2

3.5. Strengthening mechanisms

Multiple studies have found that the YS of pure metals with strong texture can be estimated assuming that different strengthening mechanisms are independent of each other:

$$\sigma_{YS} = \sigma'_0 + \sigma_{HP} + \sigma_d + \sigma_{tex} \tag{2}$$

Here, σ'_0 is the Peierls-Nabarro stress, σ_{HP} is the grain boundary or Hall-Petch (H–P) strengthening, σ_d is the dislocation strengthening and σ_{tex} is the texture strengthening. It should be noted that the dislocation strengthening can be thought of as an insignificant effect in this study, as the density of dislocations in the hot-extruded PM Al rods is at a relatively low level. Furthermore, dislocations tend to recover during the plastic deformation process due to the considerably high stacking fault energy in Al. As a result, the strengthening factors in this study can be expressed as:

$$\sigma_{YS} = \sigma_{HP} + \sigma_{tex}. \tag{3}$$

It is reported that the yield strength of a single crystal is mainly determined by the critical resolved shear stress (τ) and the Schmid factor (Ω). In the Al materials, the Ω of the <001> orientation is 0.408, while the Ω of the <111> orientation is 0.272. Correspondingly, the <001> and <111> orientations are defined as 'soft' and 'hard' orientations, respectively. Given that each grain in PM Al is an ideal single crystal, the YS of the <111> orientated grains must be always higher than the grains with <001> orientation due to the relatively lower Ω of the <111> orientation compared with the <001> orientation. Accordingly, the grains with nearly all the <111> orientations should play an important role in the texture strengthening of PM Al, which will be discussed below. It has been reported that the YS of CP Al wire induced by texture strengthening can be calculated as [5,25,29]:

$$\sigma_{tex} = \sigma_{YS} - \sigma_{HP} = \sigma_{YS} \cdot (1 - M_o / M_s) \tag{4}$$

$$M_s = f_{<111>} / \Omega_{<111>} + f_{<001>} / \Omega_{<001>} \tag{5}$$

Here, M_s is the orientation factor of CP Al wire, and $M_0 = 3.06$ is the mean orientation factor for polycrystalline Al with random orientation. In addition to a handful of γ-Al_2O_3 particles, PM Al is essentially alike to CP Al, so Eqs. (4) and (5) are appropriate for PM Al. The YSs of PM Al induced by the texture strengthening and the Hall-Petch effect were

Table 3
The average grain size, the volume fraction of the <111> texture ($f_{<111>}$) and the <001> texture ($f_{<001>}$), the orientation factor (M_s), the yield strength (σ_{YS}), the Hall-Petch effect (σ_{HP}) and the texture strengthening effect (σ_{tex}) of the hot extruded (HE) and annealed at 300 °C (HE-300) and 500 °C (HE-500) rods, cold drawn (CD) and annealed at 300 °C (CD-300) wires.

Sample	HE	HE-300	HE-500	CD	CD-300
d (μm)	1.77 ± 0.10	1.81 ± 0.13	2.91 ± 0.16	1.01 ± 0.08	1.79 ± 0.10
$f_{<111>}$	0.672	0.681	0.53	0.784	0.713
$f_{<001>}$	0.328	0.319	0.47	0.216	0.287
M_s	3.275	3.286	3.10	3.411	3.324
σ_{YS} (MPa)	105 ± 3	95 ± 2	77 ± 2	160 ± 4	89 ± 2
σ_{HP} (MPa)	98.1	88.5	76	143.5	82
σ_{tex} (MPa)	6.9	6.5	1	16.5	7

calculated, and the results are listed in Table 3.

It should be noted that only when the value of the orientation factor (M_s) is greater than the mean orientation factor ($M_0 = 3.06$), the texture can produce a significant reinforcement effect. It is demonstrated that the greatest strengthening increment (16.5 MPa) from the hard <111> texture of cold-drawn PM Al wire with the highest volume fraction of 78.4% is close to 10% of the corresponding YS (160 MPa). Additionally, the electrical conductivity of cold-drawn PM Al wires is higher than the hot-extruded PM Al rods, as seen in Fig. 11. This suggests that the change of texture component from <001> to <111> could not compromise the electrical conductivity for being unable to carse additional crystal defects during the rotation of crystallographic orientation. Therefore, as mentioned earlier [5], cold drawing can be considered as an efficient way for breaking the trade-off relation of strength and electrical conductivity for preparing the Al conductor.

It is well established that a decrease in grain size leads to an increase in strength for metals as long as the grain size is greater than a few tens of nanometers [37]. Grain refinement can effectively improve the mechanical properties of metals according to the classic Hall-Petch relationship:

$$\sigma_{HP} = \sigma_0 + kd^{-1/2} \tag{6}$$

Here, σ_{HP} is the yield stress, σ_0 is the friction stress when dislocations move on the slip plane, d is the average grain size and k is the stress concentration factor. The experimental data of the YS for the HE and cold-drawn PM Al before and after annealing is plotted against $d^{-1/2}$ in Fig. 12. Typical H–P behavior is exhibited with the slope per Eq. (6). As unanticipated, the values of the friction stress (σ_0) and the H–P slope (k) are −35 MPa and 173 MPa μm$^{1/2}$, respectively. Based on a compilation of σ_0 and k values from the previous work [5], it is revealed that both parameters are in the $\sigma_0 = 10$–61 MPa and $k = 40$–148 MPa μm$^{1/2}$ ranges for the deformed CP Al. In addition, according to the H–P relationship obtained by Hayes et al. [38], the values of σ_0 and k for the cryomilled CP Al extrusions are 250 MPa and 90 MPa μm$^{1/2}$, respectively. The σ_0 of cryomilled Al is much higher than the results summarized in Ref. [5]. All in all, the intersect values, σ_0, representing the intrinsic flow stress, are positive. However, the value of σ_0 in this study is negative, along with an increased slope. Hence, the strength-structure relationship in this investigation cannot be rationalized based on the H–P relationship. Variations in σ_0 and k may be attributed to other strengthening mechanisms that contribute to the flow stress.

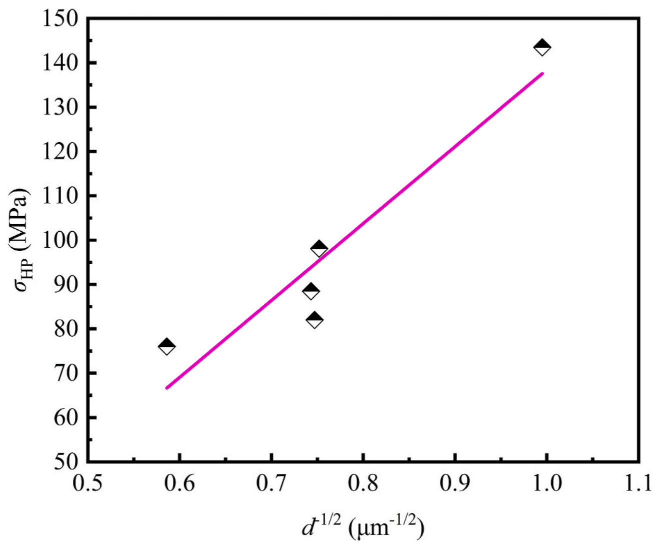

Fig. 12. Linear fitting based on the Hall-Petch equation. The YS is affected by the fine-grain strengthening (σ_{HP}) and the grain size (d) according to the Hall-Petch equation.

Based on data interpolation by Balog et al. [35], σ_0 and k are −44.8 MPa and 251.6 MPa μm$^{1/2}$, respectively. The value of σ_0 is also negative and the parameter k is significantly higher compared to the data for conventional CP Al when the mechanical tests are carried out at room temperature. Our findings are similar to these results, despite the median particle diameter of gas atomized Al powders adopted by Balog et al. being below 10 μm, finer than our raw material. Coincidentally, the average grain size in both studies falls in the 1–3 μm range, which is regarded as critical grain size (1–10 μm) to bring about a change in strengthening mechanism dominated by HAGBs [39]. The enhanced strength at critical grain size may result from the lack of mobile dislocations or easy-to-operate dislocation sources, consequently raising the flow stress independent of the grain size, and therefore leading to the increased slope (k = 173 MPa μm$^{1/2}$) [40], as seen in Fig. 12.

4. Conclusions

A novel Al conductor stabilized with a low volume fraction of γ-Al_2O_3 nanoparticles was fabricated via powder metallurgy followed by hot extrusion and cold drawing. The effects of high temperature (300 °C and 500 °C) annealing for a long time (24 h) on microstructure evolution, mechanical properties, and electrical conductivity were investigated. The following conclusions can be drawn.

- The recrystallization and grain growth of hot-extruded and cold-drawn PM Al conductors is strongly inhibited by 30–100 nm γ-Al_2O_3 dispersoids located primarily at HAGBs after annealing at 300 °C and 500 °C, thereby resulting in remarkable stabilization of the Al grain structure.
- Despite unapparent dispersion strengthening derived from the large-sized and low volume fraction γ-Al_2O_3 particles, the major contributions to the strength of PM Al conductors are due to grain refinement and texture strengthening. As the value of the friction stress (σ_0) is negative, the strength-structure relationship cannot be interpreted by the established Hall-Petch law.
- The optimal properties of PM Al wires obtained by cold drawing are the ultimate tensile strength of 172 MPa and electrical conductivity of 60.2% IACS. After annealing at 300 °C, the electrical conductivity increases to 60.8% IACS, and despite the prolonged annealing time, the yield strength of PM Al is twice as high as the CPAC.

Data availability

The raw/processed data required to reproduce these findings cannot be shared at this time as the data also forms part of an ongoing study.

CRediT authorship contribution statement

Cunguang Chen: Conceptualization, Methodology, Validation, Investigation, Resources, Writing – original draft, Visualization. **Feng Li:** Methodology, Investigation, Validation, Writing – review & editing. **Weihao Han:** Methodology, Investigation, Validation, Writing – review & editing. **Tianxing Lu:** Resources, Formal analysis, Data curation. **Pei Li:** Resources, Formal analysis, Data curation. **Qianyue Cui:** Resources, Formal analysis, Data curation. **Yanli Sui:** Methodology, Resources, Supervision, Funding acquisition. **Zhimeng Guo:** Methodology, Resources, Supervision, Funding acquisition. **Alex A. Volinsky:** Data processing and paper corrections.

Declaration of competing interest

The authors declare that they have no known competing financial interests or personal relationships that could have appeared to influence the work reported in this paper.

Acknowledgments

This work was supported by the Fundamental Research Funds for the Central Universities (FRF-GF-19-012AZ), and the State Key Lab for Advanced Metals and Materials of China (2019-Z10).

References

[1] X. Sauvage, E.V. Bobruk, M. Yu Murashkin, Y. Nasedkina, N.A. Enikeev, R. Z. Valiev, Optimization of electrical conductivity and strength combination by structure design at the nanoscale in Al-Mg-Si alloys, Acta Mater. 98 (2015) 355–366.

[2] K. Majchrowicz, Z. Pakieła, W. Chrominski, M. Kulczyk, Enhanced strength and electrical conductivity of ultrafine-grained Al-Mg-Si alloy processed by hydrostatic extrusion, Mater. Char. 135 (2018) 104–114.

[3] J.M. Hesterlee, E.T. Sanders, F.R. Thrash, Bare overhead transmission and distribution conductor design overview, IEEE Trans. Ind. Appl. 32 (3) (1996) 709–713.

[4] S. Karabay, Modification of AA-6201 alloy for manufacturing of high conductivity and extra high conductivity wires with property of high tensile stress after artificial aging heat treatment for all-aluminium alloy conductors, Mater. Des. 27 (10) (2006) 821–832.

[5] J.P. Hou, R. Li, Q. Wang, H.Y. Yu, Z.J. Zhang, Q.Y. Chen, H. Ma, X.M. Wu, X.W. Li, Z.F. Zhang, Breaking the trade-off relation of strength and electrical conductivity in pure Al wire by controlling texture and grain boundary, J. Alloys Compd. 769 (2018) 96–109.

[6] R.Z. Valiev, M.Y. Murashkin, I. Sabirov, A nanostructural design to produce high-strength Al alloys with enhanced electrical conductivity, Scripta Mater. 76 (2014) 13–16.

[7] M.Y. Murashkin, I. Sabirov, A.E. Medvedev, N.A. Enikeev, W. Lefebvre, R.Z. Valiev, X. Sauvage, Mechanical and electrical properties of an ultrafine grained Al-8.5 wt. % RE (RE = 5.4wt.% Ce, 3.1wt.% La) alloy processed by severe plastic deformation, Mater. Des. 90 (2016) 433–442.

[8] N. Kamikawa, X.X. Huang, T. Nobuhiro, N. Hansen, Strengthening mechanisms in nanostructured high-purity aluminium deformed to high strain and annealed, Acta Mater. 57 (14) (2009) 4198–4208.

[9] Y. Ito, Z. Horita, Microstructural evolution in pure aluminum processed by high-pressure torsion, Mater. Sci. Eng. 503 (1–2) (2009) 32–36.

[10] X.M. Luo, Z.M. Song, M.L. Li, Q. Wang, G.P. Zhang, Microstructural evolution and service performance of cold-drawn pure aluminum conductor wires[J], J. Mater. Sci. Technol. 33 (2017) 1039–1043.

[11] C. Yang, N. Masquellier, C. Gandiolle, X. Sauvage, Multifunctional properties of composition graded Al wires, Scripta Mater. 189 (2020) 21–24.

[12] W.H. Yuan, Z.Y. Liang, C.Y. Zhang, L.J. Wei, Effects of La addition on the mechanical properties and thermal-resistant properties of Al-Mg-Si-Zr alloys based on AA 6201, Mater. Des. 34 (2012) 788–792.

[13] W.H. Yuan, Z.Y. Liang, Effect of Zr addition on properties of Al-Mg-Si aluminum alloy used for all aluminum alloy conductor, Mater. Des. 32 (8–9) (2011) 4195–4200.

[14] W.W. Zhou, B. Cai, W.J. Li, Z.X. Liu, S. Yang, Heat-resistant Al-0.2Sc-0.04Zr electrical conductor, Mater. Sci. Eng., A 552 (2012) 353–358.

[15] J.Y. Zhang, H.X. Wang, D.Q. Yi, B. Wang, H.S. Wang, Comparative study of Sc and Er addition on microstructure, mechanical properties, and electrical conductivity of Al-0.2Zr-based alloy cables, Mater. Char. 145 (2018) 126–134.

[16] L. Liu, J.T. Jiang, B. Zhang, W.Z. Shao, L. Zhen, Enhancement of strength and electrical conductivity for a dilute Al-Sc-Zr alloy via heat treatments and cold drawing, J. Mater. Sci. Technol. 35 (6) (2019) 962–971.

[17] X.Y. Li, K. Lu, Playing with defects in metals, Nat. Mater. 16 (2017) 700–701.

[18] L. Yang, X.Y. Li, K. Lu, Making materials plain: concept, principle and applications, Acta Metall. Sin. 53 (11) (2017) 1413–1417.

[19] C.G. Chen, W.W. Wang, Z.M. Guo, C.B. Sun, A.A. Volinsky, V. Paley, Annealing effects on microstructure and mechanical properties of ultrafine-grained Al composites reinforced with nano-Al_2O_3 by rotary swaging, J. Mater. Eng. Perform. 27 (2018) 1738–1745.

[20] M. Balog, L. Orovcik, S. Nagy, P. Krizik, M. Nosko, P. Oslanec, P. Zifcak, To what extent does friction-stir welding deteriorate the properties of powder metallurgy Al? Journal of Materials Research and Technology 9 (3) (2020) 6733–6744.

[21] L. Jiang, Z.Q. Li, G.L. Fan, D. Zhang, A flake powder metallurgy approach to Al_2O_3/Al biomimetic nanolaminated composites with enhanced ductility, Scripta Mater. 65 (2011) 412–415.

[22] W.L. Zhang, Z.Q. Li, L. Jiang, X.Z. Kai, X.Y. Dai, G.L. Fan, Q. Guo, D.B. Xiong, Y. S. Su, D. Zhang, Flake thickness effect of Al_2O_3/Al biomimetic nanolaminated composites fabricated by flake powder metallurgy, Mater. Sci. Eng. 594 (2014) 324–329.

[23] Z.M. Zhang, Z. Li, Z.Q. Tan, H.T. Zhao, G.L. Fan, Y.J. Xu, D.B. Xiong, Z.Q. Li, Bioinspired hierarchical Al_2O_3/Al laminated composite fabricated by flake powder metallurgy, Composites Part A 140 (2021) 106187.

[24] M. Balog, C. Poletti, F. Simancik, M. Walcher, W. Rajner, The effect of native Al_2O_3 skin disruption on properties of fine Al powder compacts, J. Alloys Compd. 509S (2011) S235–S238.

[25] J.P. Hou, Q.Y. Chen, Q. Wang, H.Y. Yu, Z.J. Zhang, R. Li, X.W. Li, Z.F. Zhang, Effects of annealing treatment on the microstructure evolution and the strength degradation behavior of the commercially pure Al conductor, Mater. Sci. Eng. 707 (2017) 511–517.

[26] J.P. Hou, Q. Wang, H.J. Yang, X.M. Wu, C.H. Li, X.W. Li, Z.F. Zhang, Microstructure evolution and strengthening mechanisms of cold-drawn commercially pure aluminum wire, Mater. Sci. Eng. 639 (2015) 103–106.

[27] X.H. An, Q.Y. Lin, S.D. Wu, Z.F. Zhang, R.B. Figueiredo, N. Gao, T.G. Langdon, Significance of stacking fault energy on microstructural evolution in Cu and Cu-Al alloys processed by high-pressure torsion, Phil. Mag. 91 (25) (2011) 3307–3326.

[28] P. Li, S.X. Li, Z.G. Wang, Z.F. Zhang, Fundamental factors on formation mechanism of dislocation arrangements in cyclically deformed fcc single crystals, Prog. Mater. Sci. 56 (2011) 328–377.

[29] J.P. Hou, R. Li, Q. Wang, H.Y. Yu, Z.J. Zhang, Q.Y. Chen, H. Ma, X.M. Wu, X.W. Li, Z.F. Zhang, Three principles for preparing Al wire with high strength and high electrical conductivity, J. Mater. Sci. Technol. 35 (2019) 742–751.

[30] H. Park, D.N. Lee, The evolution of annealing textures in 90 pct drawn copper wire, Metall. Mater. Trans. 34 (2003) 531–541.

[31] D.N. Lee, The evolution of recrystallization textures from deformation textures, Scripta Metall. Mater. 32 (1995) 1689–1694.

[32] M. Balog, F. Simancik, M. Walcher, W. Rajner, C. Poletti, Extruded Al-Al_2O_3 composites formed in situ during consolidation of ultrafine Al powders: effect of the powder surface area, Mater. Sci. Eng. 529 (2011) 131–137.

[33] M. Balog, P. Krizik, M. Yan, F. Simancik, G.B. Schaffer, M. Qian, SAP-like ultrafine-grained Al composites dispersion strengthened with nanometric AlN, Mater. Sci. Eng. 588 (2013) 181–187.

[34] M. Balog, P. Krizik, M. Nosko, Z. Hajovska, M.V.C. Riglos, W. Rajner, D.S. Liu, F. Simancik, Forged HITEMAL: Al-based MMCs strengthened with nanometric thick Al_2O_3 skeleton, Mater. Sci. Eng. 613 (2014) 82–90.

[35] M. Balog, P. Krizik, O. Bajana, T. Hu, H. Yang, J.M. Schoenung, E.J. Lavernia, Influence of grain boundaries with dispersed nanoscale Al_2O_3 particles on the strength of Al for a wide range of homologous temperatures, J. Alloys Compd. 772 (2019) 472–481.

[36] J.H. Schneibel, M. Heilmaier, Hall-Petch breakdown at elevated temperatures, Mater. Trans. 55 (1) (2014) 44–51.

[37] K.S. Kumar, H. Van Swygenhoven, S. Suresh, Mechanical behavior of nanocrystalline metals and alloys, Acta Mater. 51 (2003) 5743–5774.

[38] R.W. Hayes, D. Witkin, F. Zhou, E.J. Lavernia, Deformation and activation volumes of cryomilled ultrafine-grained aluminum, Acta Mater. 52 (2004) 4259–4271.

[39] N. Kumar, R.S. Mishra, C.S. Huskamp, K.K. Sankaran, Critical grain size for change in deformation behavior in ultrafine grained Al–Mg–Sc alloy, Scripta Mater. 64 (2011) 576–579.

[40] K.N. Zhu, A. Godfrey, N. Hansen, X.D. Zhang, Microstructure and mechanical strength of near- and sub-micrometer grain size copper prepared by spark plasma sintering, Mater. Des. 117 (2017) 95–103.